NANO LETTERS

2007
Vol. 7, No. 1
69−74

Enhanced Charge-Collection Efficiencies and Light Scattering in Dye-Sensitized Solar Cells Using Oriented TiO_2 Nanotubes Arrays

Kai Zhu, Nathan R. Neale, Alexander Miedaner, and Arthur J. Frank*

National Renewable Energy Laboratory, Golden, Colorado 80401-3393

Received August 24, 2006; Revised Manuscript Received November 9, 2006

ABSTRACT

We report on the microstructure and dynamics of electron transport and recombination in dye-sensitized solar cells (DSSCs) incorporating oriented TiO_2 nanotube (NT) arrays. The morphology of the NT arrays, which were prepared from electrochemically anodized Ti foils, were characterized by scanning and transmission electron microscopies. The arrays were found to consist of closely packed NTs, several micrometers in length, with typical wall thicknesses and intertube spacings of 8–10 nm and pore diameters of about 30 nm. The calcined material was fully crystalline with individual NTs consisting of about 30 nm sized crystallites. The transport and recombination properties of the NT and nanoparticle (NP) films used in DSSCs were studied by frequency-resolved modulated photocurrent/photovoltage spectroscopies. While both morphologies display comparable transport times, recombination was much slower in the NT films, indicating that the NT-based DSSCs have significantly higher charge-collection efficiencies than their NP-based counterparts. Dye molecules were shown to cover both the interior and exterior walls of the NTs. Analysis of photocurrent measurements indicates that the light-harvesting efficiencies of NT-based DSSCs were higher than those found for DSSCs incorporating NPs owing to stronger internal light-scattering effects.

Dye-sensitized mesoporous nanocrystalline TiO_2 solar cells (DSSCs; also known as Grätzel cells) have received considerable attention as a potential, cost-effective alternative to silicon solar cells.[1] DSSCs feature dye molecules chemisorbed onto the surface of TiO_2 nanocrystals. The pores of the film are filled with a liquid electrolyte. Photoexcited dyes inject electrons into the TiO_2, and redox species in the electrolyte transport holes from oxidized dye molecules to the counter electrode. The injected electrons diffuse through the TiO_2 particle network to the collecting transparent conducting oxide (TCO) substrate.[2] From the light intensity dependence of the electron diffusion coefficient in randomly packed TiO_2 nanoparticle (NP) films, it has been inferred that transport is limited by the residence time of electrons in traps[3−7] and the morphology associated with both the particle network (e.g., distribution of the number of interparticle connections)[8−10] and the interparticle contact area.[11] Because the collection of photoinjected electrons competes with recombination, a high charge-collection efficiency requires that transport is significantly faster than recombination.

Films constructed of oriented one-dimensional nanostructures, such as nanotube (NT) arrays, aligned perpendicular to the collecting TCO substrate could potentially improve the charge-collection efficiency by promoting faster transport and slower recombination. The extent to which transport or recombination could be affected by an oriented architecture is expected to depend on mechanistic considerations, such as the density and location of structural defects, the crystallinity, and the composition of the redox electrolyte. Titania NTs have been prepared by several methods including electrochemical anodization,[12−15] hydrothermal synthesis,[16,17] and template-assisted synthesis.[18,19] Electrochemical anodization of Ti metal is a relatively simple approach for systematically altering the morphological properties of NT arrays, such as their pore diameter, wall thickness, intertube spacing, and tube length.[20−22] Only recently have TiO_2 NTs been incorporated into DSSCs in both oriented[23−25] and randomly packed[26−28] forms. In the case of oriented NTs, a 3.3% incident photon-to-current conversion efficiency[25] and a 3% overall conversion efficiency[23] have been reported. Transport and recombination studies on randomly packed TiO_2 NTs showed that, even with these relatively disordered systems, recombination was suppressed, while transport appeared unaffected.[28] There have been no similar studies of oriented TiO_2 NT arrays. Because transport and recombination are major determinants of the overall solar cell efficiency, study of these phenomena in oriented TiO_2 NT arrays is important for further advances in NT DSSC technology.

* To whom correspondence should be address. E-mail: afrank@nrel.gov.

10.1021/nl062000o CCC: $37.00
Published on Web 12/02/2006

In this paper, we examine the morphology and electron dynamics in TiO_2 NT arrays oriented perpendicular to a substrate. The crystal structure of a single NT and the pore density, pore diameter, wall thickness, intertube spacing, and porosity of the NT films were characterized. The transport and recombination times of electrons in NT and NP films used in DSSCs were compared. The aligned NT arrays display markedly higher charge-collection efficiencies and light-harvesting efficiencies than the traditional NP films. The photovoltaic properties of NT- and NP-based DSSCs were also studied.

Aligned TiO_2 NT arrays were prepared by electrochemically anodizing Ti foils (Alfa, 0.25 mm, 99.5% purity) in a two-electrode cell, which contained a Pt counter electrode and 0.5 wt % NH_4F in glycerol.[14] The Ti foil was biased at 20 V for 16−70 h at room temperature to produce NT arrays with lengths varying from 1.9 to 5.7 μm. The TiO_2 NT films were annealed in air at 400 °C for 3 h and stained with the N719 dye (N719 = [tetrabutylammonium]$_2$[Ru(4-carboxylic acid-4′-carboxylate-2,2′-bipyridyl)$_2$(NCS)$_2$]), using the same procedure described for NP films.[29] The amount of adsorbed N719 was measured by optical absorption of the desorbed dye as detailed previously.[29] The morphology of the NT arrays was characterized by scanning electron microscopy (SEM), transmission electron microscopy (TEM), and X-ray diffraction (XRD). Anatase TiO_2 NP paste[29] was spread on top of Ti foils via the doctor blade technique, and the resulting films were then sintered and stained using the same procedure described for the NT films. The average particle size of the sintered film was 24 nm. The NP films had thicknesses ranging from 2.5 to 7.3 μm, a surface roughness factor of 90 μm^{-1}, and a porosity of 63%.[29] The procedures for preparing semitransparent counter electrodes and for assembling DSSCs are detailed elsewhere.[29] The electrolyte was composed of 0.8 M 1-hexyl-2,3-dimethylimidazolium iodide and 50 mM iodine in methoxypropionitrile. Transport and recombination properties were measured by intensity-modulated photocurrent spectroscopy (IMPS) and intensity-modulated photovoltage spectroscopy (IMVS) as described previously.[30,31] For these measurements, the DSSCs were probed with a modulated beam of 680 nm light superimposed on a relatively large background (bias) illumination also at 680 nm. The probe and bias light entered the cell from the counter electrode side. The setup for determining the solar cell characteristics under simulated AM1.5 solar irradiance is discussed elsewhere.[29]

Morphological Characterization. Figure 1 shows typical surface and cross-sectional SEM images of as-deposited TiO_2 NT films. Nanotubes were packed in approximately hexagonal symmetry with an average inner diameter and wall thickness of 30 ± 4 and 8 ± 1 nm, respectively. The average NT lengths ranged from 1.9 to 5.7 μm as the anodization time was increased. Figure 2 compares the XRD patterns of a 2 μm thick NT film before and after annealing at a temperature of 400 °C. It can be seen that annealing transforms the as-deposited film from an amorphous material to anatase TiO_2 (identified by the (101) peak at $2\theta = 25.3°$). Selective area electron diffraction (SAED) (inset of Figure 2) also shows that the TiO_2 NTs are anatase. However, XRD measurements (not shown) of a relatively short NT array (ca. 150 nm in length), which was annealed under the same conditions, reveal the presence rutile (identified by the (110) peak at $2\theta = 27.4°$) in the barrier layer at the anatase NT−Ti substrate interface in agreement with a previous observation.[32] Applying the Scherrer equation[33] to the anatase (101) peak at $2\theta = 25.3°$ revealed an average crystallite size of 28 nm. Figure 3 displays TEM images of the same annealed NT sample. The high-resolution image of a single NT (Figure 3c) shows that the material is fully crystalline with lattice spacings of 3.52 Å, which correspond to the (101) plane. Although the average crystallite size was 28 nm as determined by XRD, Figure 3c shows that the NT walls are comprised of crystallites with lengths exceeding 50 nm. From

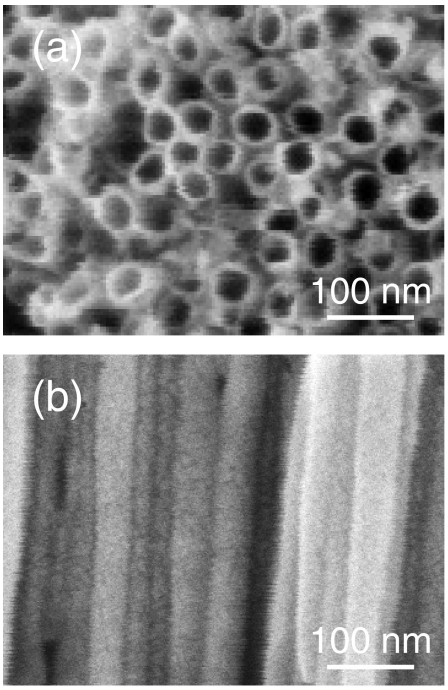

Figure 1. (a) Surface and (b) cross-sectional SEM images of as-deposited TiO_2 NTs.

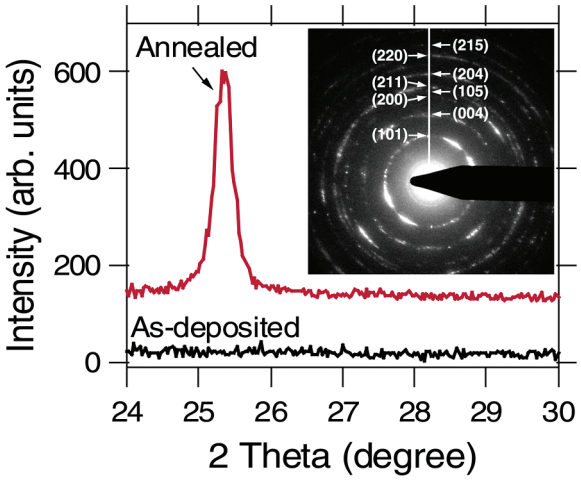

Figure 2. X-ray diffraction patterns of as-deposited and annealed TiO_2 NTs. Inset shows the SAED pattern of an annealed sample.

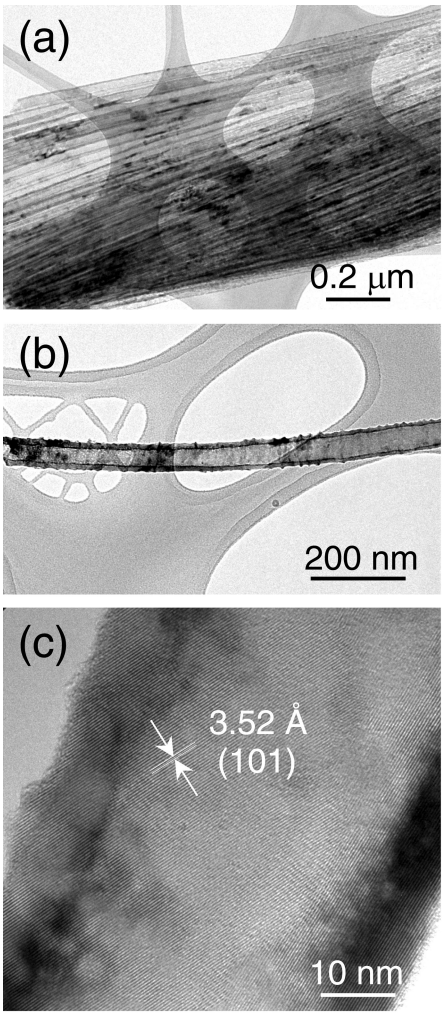

Figure 3. TEM images of annealed TiO_2 NTs. Shown are a (a) bundle, (b) single NT, and (c) high-resolution image of anatase (101) lattice spacing (3.52 Å).

geometric considerations, the surface roughness factor rf (μm^{-1}) and film porosity P of a hexagonal NT array can be determined from

$$\mathrm{rf} = \frac{2(1-P)}{w} = \frac{4\pi}{\sqrt{3}}\frac{d_p + w}{l^2} \quad (1)$$

$$P = 1 - \frac{2\pi}{\sqrt{3}}\frac{(d_p w + w^2)}{l^2} \quad (2)$$

where d_p, w, and l are the respective pore diameter, wall thickness, and center-to-center distance between NTs. From examination of SEM images in Figure 1, the average intertube spacing s appears to be comparable to the measured wall thickness w, which is also 8 ± 1 nm. For estimated d_p, w, and s values of 30, 8, and 8 nm, respectively, we determined that the center-to-center distance between NTs was 54 nm. With the aid of eq 1, we estimate a roughness factor of 94.5 μm^{-1} and a porosity of 62%.

An estimate of the roughness factor of the NT films can also be deduced from dye desorption measurements and

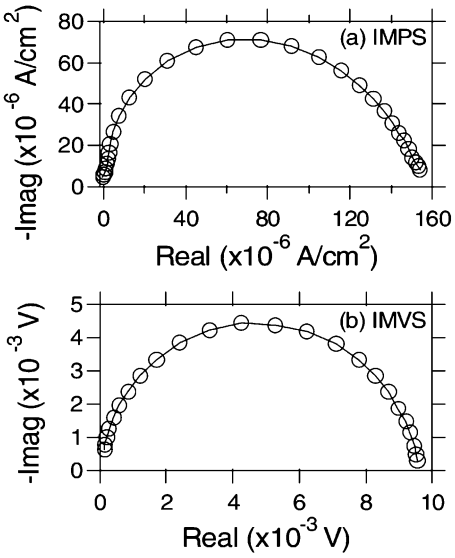

Figure 4. Typical (a) IMPS and (b) IMVS responses in the complex plane for NT-based DSSCs.

comparison with the roughness factor of the NP films. For a given film thickness, the NTs had about the same (98 ± 10%) dye loading as the NP films, suggesting that both films had comparable surface areas. From the roughness factor of the NP films (90 μm^{-1} as measured by gas sorption), we estimate that the roughness factor of the NT film was 88 ± 9 μm^{-1}, consistent with our estimate from SEM images. The comparable roughness factors suggest that dye adsorption occurs on both the interior and exterior walls of the NTs. From the experimentally determined roughness factor (88 ± 9 μm^{-1}) and wall thickness (8 ± 1 nm) of the NT array, we estimate that the film had a porosity of 65 ± 5% (eq 1) and that the average center-to-center distance between NTs was about 56 nm (eq 2), corresponding to an intertube spacing of 10 nm. From the pore diameter, wall thickness, and intertube spacing, we determined a pore density of 3.7 × 10^{10} pores/cm^2.

Transport and Recombination. Figure 4 shows typical IMPS and IMVS response curves for the TiO_2 nanotube arrays. The IMPS and IMVS plots display a semicircle in the complex plane, similar to that observed for NP cells.[7,34,35] The collection (transport) time can be estimated from the expression $\tau_c = 1/2\pi f_c$, where f_c is the characteristic frequency minimum of the IMPS imaginary component in Figure 4a. Similarly, the recombination time can be determined from $\tau_r = 1/2\pi f_r$, where f_r is the characteristic frequency minimum of the IMVS imaginary component in Figure 4b.

Figure 5 compares transport and recombination times for NT- and NP-based DSSCs as a function of the incident photon flux (light intensity) I_0. The thicknesses of the NT and NP films (4.3 and 4.2 μm, respectively) in the cells were about the same. For both film morphologies, τ_c (Figure 5a) exhibits a power-law dependence on the light intensity. For NP films, the nonlinear dependence of transport has been explained by a model in which electrons perform an exclusive random walk between trap sites that have a power-law distribution of waiting (release) times in the form of

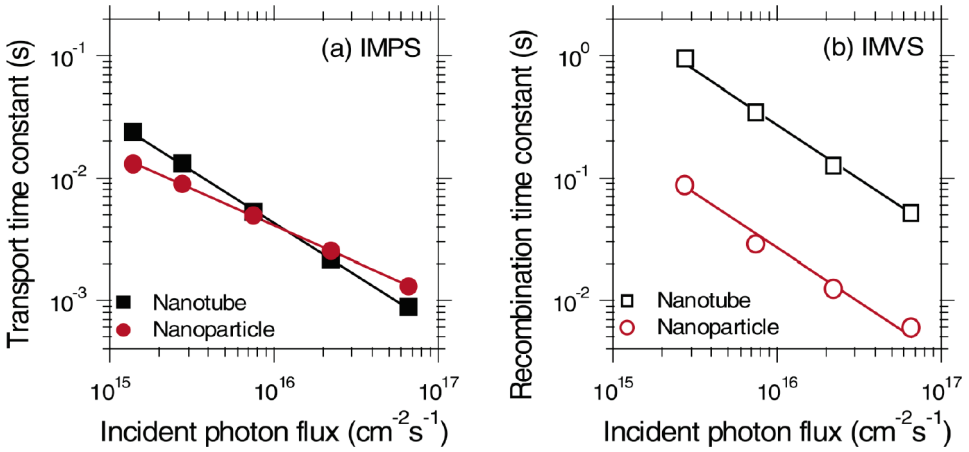

Figure 5. Comparison of (a) transport and (b) recombination time constants for NT- and NP-based DSSCs as a function of the incident photon flux for 680 nm laser illumination.

$t^{-(1+\alpha)}$, where the parameter α is related to disorder in the TiO_2 films and has values between 0 and 1.[5,8] The power-law dependence of transport on the light intensity for NT films suggests that similar mechanistic factors govern transport in NT films. It is surprising that the transport times τ_c for both film morphologies are comparable. One would have expected that transport would have been much faster in oriented NT films than in the randomly packed NP films for a given film thickness. Because the transport times τ_c and film thicknesses L for the NT and NP films are similar, it follows that the electron diffusion coefficients D for both morphologies are also similar as determined from the expression: $D = L^2/2.35\tau_c$.[8] The comparable transport times could reflect, in part, the similar average crystallite size (Figure 3c) in the NT and NP films. From the best fits of the data in Figure 5a to the expression[8] $\tau_c \propto (I_0)^{\alpha-1}$, the respective α values for NT and NP films were determined to be 0.14 and 0.40. Because the α values differ, the density and distribution of transport-limiting traps in the NT and NP films also likely vary.

Figure 5b shows that the recombination time constants τ_r for the NT arrays are an order of magnitude larger than those for the NP films over the light-intensity range investigated. The slower recombination could indicate that fewer potential surface recombination sites exist in NT arrays than in NP films. Given that recombination in the NT films is 10 times slower than that in the NP films and that the transport times for both film morphologies are about the same, the charge-collection efficiency η_{cc} for NT electrodes, as described by the relation[7] $\eta_{cc} = 1 - (\tau_c/\tau_r)$, must be significantly greater. A calculation of the charge-collection efficiency at the highest light intensity (6.6×10^{16} cm^{-2} s^{-1}) in Figure 5 shows that η_{cc} for the NT films is 25% larger than that for the NP films. It has been shown that, to a good approximation, the ratio of τ_c at short circuit and τ_r at open circuit (τ_r/τ_c) equals the ratio of the time constants measured at the maximum power point.[31] Thus, the 25% improvement in the charge-collection efficiency is close to the η_{cc} at the maximum power point. This implies that NT films can be much thicker than NP films for a given recombination loss. Therefore, NT films can be made thicker than their NP counterparts, which would allow for a higher light-harvesting efficiency, especially at the long-wavelength end of the visible and in the near-infrared region.

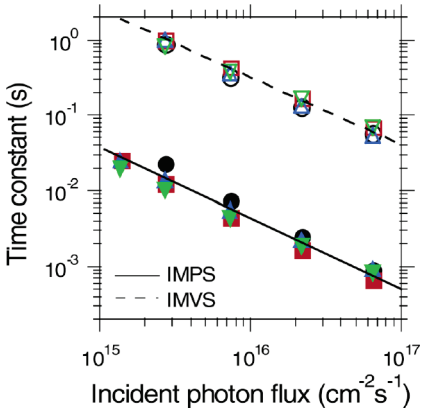

Figure 6. Transport (IMPS, solid symbols) and recombination (IMVS, open symbols) time constants for dye-sensitized NT films of various thicknesses as a function of the incident photon flux for 680 nm laser illumination. The film thicknesses are (a) 1.9 μm (●, ○), (b) 3.2 μm (■, □), (c) 4.3 μm (▲, △), and (d) 5.7 μm (▼, ▽).

Figure 6 shows the effect of film thickness on transport and recombination times for photocarriers in NT-based DSSCs. Recombination times τ_r display little, if any, dependence on the film thickness (from 1.9 to 5.7 μm), which indicates that photocarriers recombine uniformly throughout film and, consequently, that recombination losses at the TCO substrate are negligible. This latter result was not surprising given that anodization is known to generate a thin TiO_2 barrier layer[14,32] shielding the Ti substrate from direct contact with the electrolyte. What was unexpected, however, is the minimal dependence of the transport time constant τ_c on film thickness. We have shown that for NP films, the transport time τ_c is related to the film thickness as $\tau_c \propto L^{2\alpha}$ for weakly absorbed light.[8] Assuming a similar relationship for NT films, the small dependence of τ_c on film thickness could be related to the small α value ($\alpha = 0.14$) such that when L is increased by a factor of 3, τ_c only increases by 36%.

Figure 7 shows the short-circuit photocurrent density J_{sc} dependences of the NT and NP films on film thickness at 680-nm illumination. The incident photon flux I_0 was held

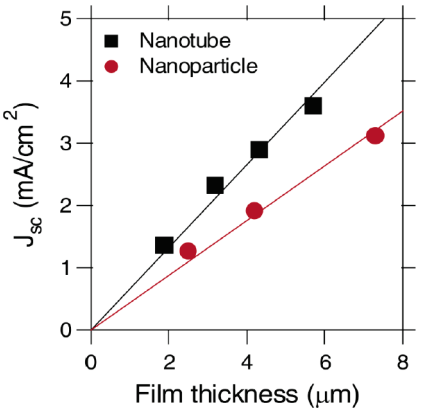

Figure 7. Comparison of the short-circuit photocurrent densities of dye-sensitized NT and NP cells as a function of film thickness. The cells were illuminated by a 680-nm laser with an incident photon flux of 6.6×10^{16} cm^{-2} s^{-1}. Lines represent linear fits of data.

constant at 6.6×10^{16} cm^{-2} s^{-1}. The photocurrent density is seen to increase linearly with the thickness of both NT and NP films. However, the rate of increase of J_{sc} with L is larger for the NT films than for the NP films. In general, J_{sc} can be approximated by the expression

$$J_{sc} = q\eta_{lh}\eta_{inj}\eta_{cc}I_0 \quad (3)$$

where q is the elementary charge, η_{lh} is the light-harvesting efficiency of a cell, and η_{inj} is the charge-injection efficiency. The product of η_{lh}, η_{inj}, and η_{cc} is commonly referred to as the incident photon-to-current conversion efficiency. Of the three parameters, η_{lh} is determined by the amount of adsorbed dye, which is proportional to the film thickness for weakly absorbed light (as is the case for 680-nm illumination), the light-scattering properties of the film, the concentration of redox species, and other factors;[36] η_{cc} is largely determined by the competition between recombination and charge collection;[7] η_{inj} values of adsorbed N719 on the TiO_2 NTs and NPs were assumed to be the same. Inasmuch as NT and NP films have comparable dye coverage and are exposed to the same redox electrolyte, the slopes of the plots of J_{sc} vs film thickness are primarily determined by η_{cc} and the light-scattering properties of the films. The ratio of slopes of the plots for the respective NT and NP films is 1.5 ± 0.1, which implies that the product of $\eta_{lh}\eta_{cc}$ for the NT films is about 50% larger than that for the NP films. From the measured $\eta_{lh}\eta_{cc}$ and η_{cc} values, one can estimate the difference in η_{lh} between the NT and NP films. As discussed above, the 25% improvement in the charge-collection efficiency is close to the expected η_{cc} at the maximum power point and likely represents an upper limit of the difference in charge-collection efficiencies between the NT and NP films at short circuit.[31] From the respective 50% and 25% values of $\eta_{lh}\eta_{cc}$ and η_{cc}, we estimate that η_{lh} of NT films is at least 20% larger than that of NP films at short circuit. Considering the comparable dye coverage and redox electrolyte composition, we attribute the increased η_{lh} to enhanced internal light scattering in the NT films with respect to that in the NP films. The latter observation concurs with a recent study comparing the light-scattering properties of TiO_2 NT and NP films.[37]

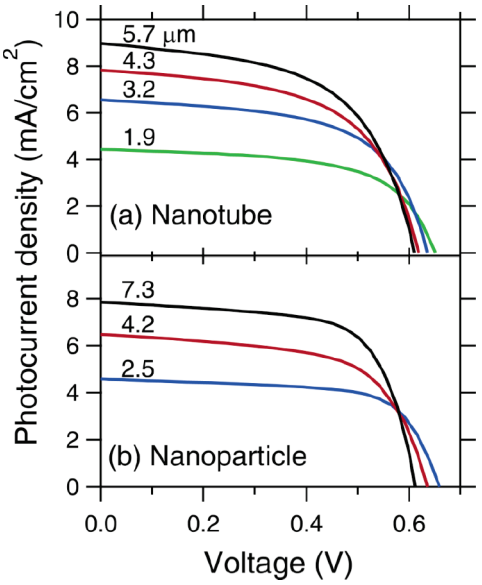

Figure 8. $J-V$ characteristics of dye-sensitized (a) NT and (b) NP solar cells as a function of film thickness under simulated AM1.5 light.

Table 1. $J-V$ Characteristics of Dye-Sensitized NT and NP Solar Cells under Simulated AM1.5 Light

film type	L (μm)	J_{sc} (mA/cm^2)	V_{oc} (V)	FF	η (%)
NT	1.9	4.4	0.64	0.60	1.7
	3.2	6.6	0.63	0.58	2.4
	4.3	7.8	0.61	0.57	2.7
	5.7	9.0	0.61	0.55	3.0
NP	2.5	4.6	0.65	0.69	2.1
	4.2	6.5	0.63	0.63	2.6
	7.3	7.9	0.61	0.66	3.2

Solar Cell Performance. Figure 8 and Table 1 compare the photocurrent density−voltage ($J-V$) properties of NT- and NP-based DSSCs as a function of film thicknesses under simulated AM1.5 light. At comparable film thicknesses (e.g., ca. 4.2 μm), the photocurrent densities of the NT-based DSSCs are larger than those of NP-based DSSCs while there are essentially no substantial differences in the photovoltages. On the basis of the much longer photoelectron lifetime τ_r (Figure 5b) and the greater J_{sc} (Table 1) observed for NT-based DSSCs, one might expect that the larger photoelectron densities n ($n \propto J_{sc}\tau_r$)[30] would give rise to a higher V_{oc}.[36] However, because of the distinct morphologies, the electronic properties of the NT and NP films are likely to be different. Indeed, the disorder parameters of the NT and NP films were found to differ significantly. As discussed in connection with Figure 5a, the respective α values for NT and NP films are 0.14 and 0.40. These numbers imply that the density of states in the NT films is larger than that in the NP films. Consequently, for the same V_{oc}, the NT films require a larger photoelectron density than NP films. Also, the fill factors (FF) of the NT-based DSSCs are slightly lower than those of NP-based DSSCs for comparable film thicknesses. In view

of the observation that an insulating oxide layer forms between the NTs and the substrate during anodization process,[14,32] we attribute the lower *FF* to a larger series (sheet) resistance at the NT/substrate interface. The lower fill factor of the NT-based DSSCs offsets the gain in J_{sc} resulting in both NT- and NP-based DSSCs having essentially the same solar conversion efficiencies.

In conclusion, we investigated the morphology and electron dynamics of oriented TiO_2 NT arrays prepared from electrochemically anodizing Ti foils. The average NT inner diameter and wall thickness were 30 and 8 nm, respectively. The calcined NTs were fully crystalline with the anatase (101) crystal plane comprising most of the surface. The average NT crystallite size was 28 nm, although much longer grains were observed. Dye molecules were shown to cover the interior and exterior NT walls. As in the case of NP films, the electron transport and recombination times for the NT films display power-law dependences on the incident light intensity. For a given film thickness, the NT and NP films had similar transport times, whereas recombination was 10 times slower in the NT films, indicating that the charge-collection efficiency of the NT photoelectrodes was markedly enhanced. Higher light-harvesting efficiencies were observed for NT-based DSSCs because of stronger light scattering effects. The photocurrent densities of NT-based DSSCs were higher than those of NP-based DSSCs, while their photovoltages were comparable. Finally, varying the electrochemical fabrication conditions is known[14,20] to affect the geometry and surface properties of the NT arrays. Investigations of the consequences of these morphological changes on the photoconversion processes are likely to improve significantly the photoconversion efficiencies of NT-based DSSCs.

Acknowledgment. This work was supported by the Office of Science, Division of Chemical Sciences, and the Office of Utility Technologies, Division of Photovoltaics, U.S. Department of Energy, under Contract DE-AC36-99GO10337.

References

(1) O'Regan, B.; Grätzel, M. *Nature* **1991**, *353*, 737.
(2) Kopidakis, N.; Schiff, E. A.; Park, N. G.; van de Lagemaat, J.; Frank, A. J. *J. Phys. Chem. B* **2000**, *104*, 3930.
(3) Cao, F.; Oskam, G.; Meyer, G. J.; Searson, P. C. *J. Phys. Chem.* **1996**, *100*, 17021.
(4) de Jongh, P. E.; Vanmaekelbergh, D. *Phys. Rev. Lett.* **1996**, *77*, 3427.
(5) Nelson, J.; Haque, S. A.; Klug, D. R.; Durrant, J. R. *Phys. Rev. B* **2001**, *63*, 205321.
(6) Dloczik, L.; Ileperuma, O.; Lauermann, I.; Peter, L. M.; Ponomarev, E. A.; Redmond, G.; Shaw, N. J.; Uhlendorf, I. *J. Phys. Chem. B* **1997**, *101*, 10281.
(7) Schlichthörl, G.; Park, N. G.; Frank, A. J. *J. Phys. Chem. B* **1999**, *103*, 782.
(8) van de Lagemaat, J.; Frank, A. J. *J. Phys. Chem. B* **2001**, *105*, 11194.
(9) Benkstein, K. D.; Kopidakis, N.; van de Lagemaat, J.; Frank, A. J. *J. Phys. Chem. B* **2003**, *107*, 7759.
(10) Kopidakis, N.; Benkstein, K. D.; van de Lagemaat, J.; Frank, A. J.; Yuan, Q.; Schiff, E. A. *Phys. Rev. B* **2006**, *73*, 045326.
(11) Cassiers, K.; Linssen, T.; Mathieu, M.; Bai, Y. Q.; Zhu, H. Y.; Cool, P.; Vansant, E. F. *J. Phys. Chem. B* **2004**, *108*, 3713.
(12) Gong, D.; Grimes, C. A.; Varghese, O. K.; Hu, W. C.; Singh, R. S.; Chen, Z.; Dickey, E. C. *J. Mater. Res.* **2001**, *16*, 3331.
(13) Mor, G. K.; Varghese, O. K.; Paulose, M.; Grimes, C. A. *Adv. Funct. Mater.* **2005**, *15*, 1291.
(14) Macak, J. M.; Tsuchiya, H.; Taveira, L.; Aldabergerova, S.; Schmuki, P. *Angew. Chem., Int. Ed.* **2005**, *44*, 7463.
(15) Beranek, R.; Hildebrand, H.; Schmuki, P. *Electrochem. Solid State Lett.* **2003**, *6*, B12.
(16) Kasuga, T.; Hiramatsu, M.; Hoson, A.; Sekino, T.; Niihara, K. *Langmuir* **1998**, *14*, 3160.
(17) Chen, Q.; Zhou, W. Z.; Du, G. H.; Peng, L. M. *Adv. Mater.* **2002**, *14*, 1208.
(18) Hoyer, P. *Langmuir* **1996**, *12*, 1411.
(19) Sander, M. S.; Cote, M. J.; Gu, W.; Kile, B. M.; Tripp, C. P. *Adv. Mater.* **2004**, *16*, 2052.
(20) Cai, Q. Y.; Paulose, M.; Varghese, O. K.; Grimes, C. A. *J. Mater. Res.* **2005**, *20*, 230.
(21) Mor, G. K.; Shankar, K.; Paulose, M.; Varghese, O. K.; Grimes, C. A. *Nano Lett.* **2005**, *5*, 191.
(22) Paulose, M.; Shankar, K.; Yoriya, S.; Prakasam, H. E.; Varghese, O. K.; Mor, G. K.; Latempa, T. A.; Fitzgerald, A.; Grimes, C. A. *J. Phys. Chem. B* **2006**, *110*, 16179.
(23) Mor, G. K.; Shankar, K.; Paulose, M.; Varghese, O. K.; Grimes, C. A. *Nano Lett.* **2006**, *6*, 215.
(24) Paulose, M.; Shankar, K.; Varghese, O. K.; Mor, G. K.; Hardin, B.; Grimes, C. A. *Nanotechnology* **2006**, *17*, 1446.
(25) Macak, J. M.; Tsuchiya, H.; Ghicov, A.; Schmuki, P. *Electrochem. Commun.* **2005**, *7*, 1133.
(26) Adachi, M.; Murata, Y.; Okada, I.; Yoshikawa, S. *J. Electrochem. Soc.* **2003**, *150*, G488.
(27) Uchida, S.; Chiba, R.; Tomiha, M.; Masaki, N.; Shirai, M. *Electrochemistry* **2002**, *70*, 418.
(28) Ohsaki, Y.; Masaki, N.; Kitamura, T.; Wada, Y.; Okamoto, T.; Sekino, T.; Niihara, K.; Yanagida, S. *Phys. Chem. Chem. Phys.* **2005**, *7*, 4157.
(29) Neale, N. R.; Kopidakis, N.; van de Lagemaat, J.; Grätzel, M.; Frank, A. J. *J. Phys. Chem. B* **2005**, *109*, 23183.
(30) Schlichthörl, G.; Huang, S. Y.; Sprague, J.; Frank, A. J. *J. Phys. Chem. B* **1997**, *101*, 8141.
(31) van de Lagemaat, J.; Park, N. G.; Frank, A. J. *J. Phys. Chem. B* **2000**, *104*, 2044.
(32) Varghese, O. K.; Gong, D. W.; Paulose, M.; Grimes, C. A.; Dickey, E. C. *J. Mater. Res.* **2003**, *18*, 156.
(33) Park, N. G.; Schlichthörl, G.; van de Lagemaat, J.; Cheong, H. M.; Mascarenhas, A.; Frank, A. J. *J. Phys. Chem. B* **1999**, *103*, 3308.
(34) Fisher, A. C.; Peter, L. M.; Ponomarev, E. A.; Walker, A. B.; Wijayantha, K. G. U. *J. Phys. Chem. B* **2000**, *104*, 949.
(35) Franco, G.; Gehring, J.; Peter, L. M.; Ponomarev, E. A.; Uhlendorf, I. *J. Phys. Chem. B* **1999**, *103*, 692.
(36) Frank, A. J.; Kopidakis, N.; van de Lagemaat, J. *Coord. Chem. Rev.* **2004**, *248*, 1165.
(37) Ma, Y. T.; Lin, Y. A.; Xiao, X. R.; Li, X. P.; Zhou, X. W. *Chin. Sci. Bull.* **2005**, *50*, 1985.

NL062000O